Multi-frequency averaging (MFA) model of a generic electric vehicle powertrain suitable under variable frequency of averaging developed for remote operability

Surojit Sen[1] ✉, Paul L. Evans[1], C. Mark Johnson[1]

[1]*Power Electronics Machines and Control (PEMC) Group, Department of Electrical and Electronics Engineering, University of Nottingham, Nottingham, UK*

✉ *E-mail: surojit.sen1@nottingham.ac.uk*

Abstract: Geographically distributed hardware-in-the-loop (HIL) testing has the potential to allow hybrid vehicle powertrain components (battery, motor drive, and engine) to be developed at geographically remote locations but tested concurrently and coupled. Inter-location internet communication links can allow non-ideal behaviour observed in a physical component in one location (e.g. an electrical drive) to be imposed on another physical component elsewhere (e.g. an ICE), and vice-versa. A key challenge is how to represent the behaviour of a remote, physical component under testing in a local HIL environment. Internet communications are too slow and unreliable to transmit waveforms in real-time and so one solution is to use a local 'slave' model whose behaviour and parameters are tuned based on observations at the remote location. This study proposes a multi-frequency averaging (MFA) slave model of an electric motor drive system for use in this application; it addresses a weakness in previously published work by extending the MFA model to variable frequency operation. The model was benchmarked against experimental operation (and its equivalent simulation model) in open-loop and closed-loop space vector pulse-width modulation control strategy, fixed and variable frequency operation. Results show significant reconciliation of model and experiment.

1 Introduction

The modern automotive industry has increasingly shifted to electrified powertrains in the quest for environmental sustainability. The newer hybrid/electric units have many sub-systems working together, and each needs to complement the others to become a single unit performing optimally. For example, the battery design configuration should be matched precisely with the inverter unit or the motor output should be matched with the engine mechanically for the whole system to operate reliably over its lifetime. Ideally, all sub-systems are co-located for system prototype testing all throughout its development, but this is expensive and time-consuming especially for the automotive industry since they are usually developed under different roofs and often by different companies/suppliers who are bound by confidentiality clauses.

Hardware-in-the-loop (HIL) testing has helped by allowing a single sub-system prototype to be loaded by the test-rig which behaves as the remainder of the system. On-going work is looking to extend this to couple multiple sub-system HIL rigs in real-time that ideally removes the pre-requisite for co-location in order to do a full system optimisation test. The key challenge is that readily available communication links (to link the HIL rigs) such as the internet have unpredictable and uncontrollable bandwidth and latency, effectively making real-time transmission of sub-system outputs impossible.

A potential solution is to have a 'slave' model representing every sub-system in the location where it is not physically present and be periodically re-aligned to proxy the master behaviour as accurately as the communication medium allows. Suitable slave models must be, therefore, developed for all sub-systems that can model baseline behaviour accurately and also accept 're-alignment directives' from a remote location. This work focuses on the development and validation of the said 'slave' model for an electric-drive sub-system.

Understanding the requirements more closely; the remote slave model of a generic e-drive device-under-test must faithfully reproduce the local HIL baseline behaviour and also be compliant with its erratic behaviour and shifting operating region as one-off

outlier events every now and then through re-alignment packets. Secondly, real-time operation indicates there is a cost associated with complex models. Thirdly, information on one-off events such as outliers and shifting operating regions can be propagated only as fast as communication medium allows that might have unintended consequences on the global stability of system simulation. Lastly, the presence of jitter requires re-sequencing of received re-alignment packets.

It was quickly understood that for electrical systems, exchanging signals in frequency-domain (i.e. amplitudes of harmonics of interest as a function of time or dynamic phasors) is advantageous since although the variables change rapidly, their component phasors are slow and specific. This helps by reducing the system time constants (increasing simulation speed) and reducing the sensitivity of waveform reproduction accuracy on communication delays. Secondly, different variables may be needed in different levels of fidelity, i.e. only DC component for rotor speed but several harmonics of motor current may be needed to compute switching losses. Also, minimal model complexity is needed for real-time simulation. These three requirements led to the identification of multi-frequency averaging (MFA; terminology interchangeably used with generalised average modelling and dynamic phasors in the research community) as the underlying methodology for the remote observer model of an automotive e-powertrain.

Most works in the field were found to be of either fixed-frequency operation or without in-depth experimental validation and analysis. A recent work [1] by the authors has introduced the motivation behind using MFA for the remote observer model of a generic e-powertrain and validated its variable frequency operation against high-fidelity switching model simulation results. This study builds on it by benchmarking an improved MFA model against experimental results from an e-drive (originally designed for a racing car) running space vector pulse-width modulation (SVPWM) control with third harmonic injection. An equivalent high-fidelity switching model was developed to replicate the hardware that was used for further benchmarking studies with
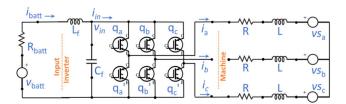
Fig. 1 *Generic electric vehicle powertrain (battery, LC filter, power converter, AC machine)*

controlled conditions, not achievable under experimental conditions.

The paper is structured as follows: a literature review of MFA is followed by modelling methodology, which covers the mathematical aspect of MFA. The validation methodology follows that looks at the experimental setup and its equivalent simulation model. Benchmarking studies and results follow with conclusions marking the end of the paper.

2 MFA review

Power converters today use very high speed switches (ranging from a few hundred kHz for insulated gate bipolar transistor (IGBT) to MHz scale for wide-bandgap devices [2]) to control the power flow between AC and DC. While, on the one hand, higher switching frequency results in faster transient response and smaller magnetic circuits, more switching actions reduce efficiency via switching losses as every device spends more energy transitioning between on and off states [3]. Either way, real-time switching models are very difficult even with the fastest processors of today and many electromagnetic and thermal applications require switching behaviour to be modelled. Owing to the non-linearity and time-variance of switching devices, modellers are compelled to either approximate to linear time-invariant systems in an operation region; or use newer non-linear or hybridised methodologies that are sluggish. Frances *et al.* [4] provided a comprehensive review of power converter modelling covering the whole spectrum of methodologies for DC microgrid applications.

High complexity and slow simulation of detailed switching models limit their utility to non-real-time cases only. Averaged models, on the other hand, are simple and quick [5]. State-space-averaging (SSA) describes the system state in each switch mode (i.e. there are eight modes in a six-switch full bridge) by averaging the variables over a switching cycle by weighting the modes with their respective duties [6, 7]. Conditions, where the averaging frequency is well below switching frequency and duty cycle, are relatively constant over an averaging period where SSA outperforms. A stationary motor application, such as diesel generators, is a good example.

Automotive traction application is different from the above owing to dynamic torque demand and variable frequency of operation. Moreover, SSA is unable to compute switching ripples or their cross-coupling effects [8]. MFA performs well if the minimum computation requirement is preferred [9]. MFA is a generalisation of SSA (hence also called generalised average modelling) in which the variables are represented by a sum of sinusoids of different frequencies (in addition to the mean DC value) averaged over the same fundamental period; can include any number of harmonics to improve waveform fidelity at the cost of incremental simulation run-time. Fourier series ((1) and (2)) is used to break-down a quasi-periodic function into an infinite sum of orthogonal sines and cosines with the reproduction accuracy increasing by including more sinusoids. This works quite well for pulse-width modulation (PWM)-converter current waveforms since these are essentially sinusoidal fundamental with switching ripple sinusoids at various higher harmonic frequencies and sidebands around them.

$$x(t) = \sum_{k=-n}^{n} \langle x \rangle_k(t) \mathrm{e}^{\mathrm{j}k\omega t} \tag{1}$$

where index k refers to the kth harmonic content

$$\langle x \rangle_k(t) = \frac{1}{T} \int_{t-T}^{t} x(\tau) \mathrm{e}^{-\mathrm{j}k\omega\tau} \, \mathrm{d}\tau \tag{2}$$

MFA has lately been chosen in many power converter modelling applications having demonstrated a good degree of accuracy with detailed switching models and experimental results but at a fraction of computation cost. Lin and Ma [10] performed a detailed work on a three-phase full-bridge converter running a three-phase load and effect of dead-time incorporated. A similar work from the University of Kentucky [11] derived the MFA models for single- and three-phase converters and observes the effects of including specific sidebands on overall accuracy. The MFA method can be extended to account for the harmonics produced by various modulation schemes, another work from the same authors [12] have developed the mathematics for sinusoidal modulation with third harmonic injection. Bhejati *et al.* [8] derived MFA models for PWM-switching functions for different forms of the carrier signal in use today (sawtooth and isosceles triangle).

The mathematical framework developed in [11, 12] has been re-used in this study, with an extension into variable frequency operation.

3 Modelling methodology

3.1 State–space system

A generic electric powertrain is shown (Fig. 1). Traction battery (variable voltage source and internal resistance) with input inductor–capacitor (LC) filter on the DC-side of a full-bridge power converter, drives a three-phase round rotor AC synchronous machine. This is defined by the state–space model

$$\frac{\mathrm{d}}{\mathrm{d}t} i_{\mathrm{batt}} = \frac{1}{L_{\mathrm{f}}} v_{\mathrm{batt}} - \frac{R_{\mathrm{batt}}}{L_{\mathrm{f}}} i_{\mathrm{batt}} - \frac{1}{L_{\mathrm{f}}} v_{\mathrm{in}} \tag{3}$$

$$\frac{\mathrm{d}}{\mathrm{d}t} v_{\mathrm{in}} = \frac{1}{C_{\mathrm{f}}} i_{\mathrm{batt}} - \frac{1}{C_{\mathrm{f}}} i_{\mathrm{in}} \tag{4}$$

$$i_{\mathrm{in}} = q_a i_a + q_b i_b + q_c i_c \tag{5}$$

$$v_{a,b,c} = v_{\mathrm{in}}\left(\frac{2}{3} q_{a,b,c} - \frac{1}{3} q_{b,a,c} - \frac{1}{3} q_{c,a,b}\right) \tag{6}$$

$$\frac{\mathrm{d}}{\mathrm{d}t} i_{a,b,c} = \frac{1}{L} v_{a,b,c} - \frac{R}{L} i_{a,b,c} - \frac{1}{L} vs_{a,b,c} \tag{7}$$

3.2 MFA theoretical foundation

The above system of equations can be solved for frequency-domain counterparts (i.e. amplitudes of its component sinusoids) of the state variables. A time-domain variable x is represented by $\boldsymbol{X}$, a vector of its Fourier coefficients (8) where every frequency component is represented by the index pair (n, i)

$$x(t) \simeq \begin{bmatrix} 1 & \cdots & \cos(n\hat{\omega} + i\bar{\omega})t & \sin(n\hat{\omega} + i\bar{\omega})t & \cdots \end{bmatrix} \times \begin{bmatrix} X_{0,0} \\ \vdots \\ X_{n,ic} \\ X_{n,is} \\ \vdots \end{bmatrix} \tag{8}$$

$$= \boldsymbol{C}(t) \times \boldsymbol{X}(t)$$

Using (8) for the fundamental and switching frequency harmonics and differentiating, i.e. $(n, i) \in \{(0, 1), (1, 0)\}$ as an example
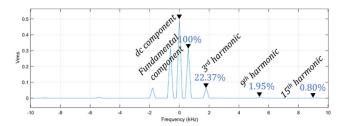
Fig. 2 *Spectral analysis of modulating signal from actual hardware shows the different active harmonics*
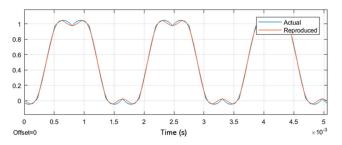

Fig. 3 *Comparison of the modulation signal from the actual hardware and MFA simulation using only the fundamental and third harmonic content*

$$x(t) \simeq \begin{bmatrix} 1 & \cos \bar{\omega}t & \sin \bar{\omega}t & \cos \hat{\omega}t & \sin \hat{\omega}t \end{bmatrix} \times \begin{bmatrix} X_{0,0} \\ X_{0,1c} \\ X_{0,1s} \\ X_{1,0c} \\ X_{1,0s} \end{bmatrix} \quad (9)$$

$$= \boldsymbol{C}(t) \times \boldsymbol{X}(t)$$

Differentiating

$$\frac{\mathrm{d}x}{\mathrm{d}t} = \frac{\mathrm{d}\boldsymbol{C}(t)}{\mathrm{d}t}\boldsymbol{X} + \boldsymbol{C}(t)\frac{\mathrm{d}\boldsymbol{X}(t)}{\mathrm{d}t}$$

$$\simeq \begin{bmatrix} 1 & \cos \bar{\omega}t & \sin \bar{\omega}t & \cos \hat{\omega}t & \sin \hat{\omega}t \end{bmatrix}$$

$$\times \left(\begin{bmatrix} 0 & 0 & 0 & 0 & 0 \\ 0 & 0 & \bar{\omega} & 0 & 0 \\ 0 & -\bar{\omega} & 0 & 0 & 0 \\ 0 & 0 & 0 & 0 & \hat{\omega} \\ 0 & 0 & 0 & -\hat{\omega} & 0 \end{bmatrix} \times \begin{bmatrix} X_{0,0} \\ X_{0,1c} \\ X_{0,1s} \\ X_{1,0c} \\ X_{1,0s} \end{bmatrix} + \begin{bmatrix} \dot{X}_{0,0} \\ \dot{X}_{0,1c} \\ \dot{X}_{0,1s} \\ \dot{X}_{1,0c} \\ \dot{X}_{1,0s} \end{bmatrix} \right) \quad (10)$$

$$\simeq \boldsymbol{C}(t)\left(\boldsymbol{T}\boldsymbol{X}(t) + \frac{\mathrm{d}\boldsymbol{X}(t)}{\mathrm{d}t} \right)$$

$\boldsymbol{T}$ can be similarly computed for higher orders to deduce a generic form. The process of multiplication in time-domain translates to convolution in frequency-domain, derivation of which could be found in [13]. Cross-coupling of frequencies occurs during convolution that leads to new harmonics emerging in the form of sums and differences of convoluting harmonics. It is up to the modeller's discretion as to which new frequencies should be retained.

The system equations (3)–(7) can be transformed to the following:

$$\frac{\mathrm{d}}{\mathrm{d}t}\boldsymbol{I}_{\mathrm{batt}} = \frac{1}{L_{\mathrm{f}}}\boldsymbol{V}_{\mathrm{batt}} - \left(\frac{R_{\mathrm{batt}}}{L_{\mathrm{f}}} + \boldsymbol{T} \right)\boldsymbol{I}_{\mathrm{batt}} - \frac{1}{L_{\mathrm{f}}}\boldsymbol{V}_{\mathrm{in}} \quad (11)$$

$$\frac{\mathrm{d}}{\mathrm{d}t}\boldsymbol{V}_{\mathrm{in}} = \frac{1}{C_{\mathrm{f}}}\boldsymbol{I}_{\mathrm{batt}} - \frac{1}{C_{\mathrm{f}}}\boldsymbol{I}_{\mathrm{in}} - \boldsymbol{T}\boldsymbol{V}_{\mathrm{in}} \quad (12)$$

$$\boldsymbol{I}_{\mathrm{in}} = \boldsymbol{Q}_a \otimes \boldsymbol{I}_a + \boldsymbol{Q}_b \otimes \boldsymbol{I}_b + \boldsymbol{Q}_c \otimes \boldsymbol{I}_c \quad (13)$$

$$\boldsymbol{V}_{a,b,c} = \boldsymbol{V}_{\mathrm{in}} \otimes \left(\frac{2}{3}\boldsymbol{Q}_{a,b,c} - \frac{1}{3}\boldsymbol{Q}_{b,a,c} - \frac{1}{3}\boldsymbol{Q}_{c,a,b} \right) \quad (14)$$

$$\frac{\mathrm{d}}{\mathrm{d}t}\boldsymbol{I}_{a,b,c} = \frac{1}{L}\boldsymbol{V}_{a,b,c} - \left(\frac{R}{L} + \boldsymbol{T} \right)\boldsymbol{I}_{a,b,c} - \frac{1}{L}\boldsymbol{Vs}_{a,b,c} \quad (15)$$

where vector $\boldsymbol{X}$ is defined as

$$\boldsymbol{X} = \begin{bmatrix} X_{0,0} \\ \vdots \\ X_{n,ic} \\ X_{n,is} \\ \vdots \end{bmatrix}$$

and

$$\boldsymbol{X} \in \left\{ \begin{array}{l} \boldsymbol{I}_{\mathrm{batt}}, \boldsymbol{V}_{\mathrm{batt}}, \boldsymbol{V}_{\mathrm{f}}, \boldsymbol{I}_{\mathrm{f}}, \boldsymbol{V}_a, \boldsymbol{V}_b, \boldsymbol{V}_c, \boldsymbol{Q}_a, \boldsymbol{Q}_b, \boldsymbol{Q}_c, \\ \boldsymbol{I}_a, \boldsymbol{I}_b, \boldsymbol{I}_c, \boldsymbol{Vs}_a, \boldsymbol{Vs}_b, \boldsymbol{Vs}_c \end{array} \right\}$$

3.3 Switching function

As discussed before, an Infineon™-sourced AC drive with custom control logic and SVPWM modulation was used as a benchmark for validation. The modulation signal for open-loop control (fixed voltage phasor and frequency) was observed from its equivalent simulation model (Figs. 2 and 3). Spectral analysis shows a sinusoidal modulation strategy with a third-harmonic injection of 22.37% amplitude. Fourier representation of the PWM signal generated for this modulation signal has been shown to be of the form (16) in [12]

$$\begin{aligned} q(t) &= q_{0,0} + q_{0,1c}\cos \bar{\omega}t + q_{0,1s}\sin \bar{\omega}t \\ &\quad + q_{0,3c}\cos 3\bar{\omega}t + q_{0,3s}\sin 3\bar{\omega}t \\ &\quad + \sum_{n=1}^{\infty}\sum_{i=-\infty}^{\infty} q_{n,ic}\cos(n\hat{\omega}t + i\bar{\omega}t) \\ &\quad + \sum_{n=1}^{\infty}\sum_{i=-\infty}^{\infty} q_{n,is}\sin(n\hat{\omega}t + i\bar{\omega}t) \end{aligned} \quad (16)$$

The signal has a DC component of 0.5 and each sinusoid is broken into a pair of sine and cosine. The values of coefficients are covered in the original source [12]. Indices (n, i) signify the order of carrier and fundamental frequency in the harmonic. The MFA model is set up on this scheme: a pair of (n, i) identifying a frequency component (k) and the modeller can choose more pairs for increased fidelity but at the cost of increased simulation time.

3.4 Variable frequency operation

In (8), a time-varying variable is dissociated into a fixed set of frequency components (DC, fundamental, and harmonics) and their time-varying amplitudes (dynamic phasors). A sinusoid $\cos \bar{\omega}t$ is in effect $\cos \theta$, with $\theta = \bar{\omega}t$. For time-varying frequency, this relation does not hold true and must be replaced with

$$\bar{\theta} = \int_{t-\tau}^{t} \bar{\omega}\,\mathrm{d}\tau \quad (17)$$

Applying this change and following the mathematics in (9) and (10) for the index pairs $(n, i) \in \{(0, 1), (1, 0)\}$ as an example

$$x(t) \simeq \begin{bmatrix} 1 & \cos \bar{\theta}(t) & \sin \bar{\theta}(t) & \cos \hat{\theta}(t) & \sin \hat{\theta}(t) \end{bmatrix} \times \begin{bmatrix} X_{0,0} \\ X_{0,1c} \\ X_{0,1s} \\ X_{1,0c} \\ X_{1,0s} \end{bmatrix} \quad (18)$$

$$= \boldsymbol{C}(t) \times \boldsymbol{X}(t)$$

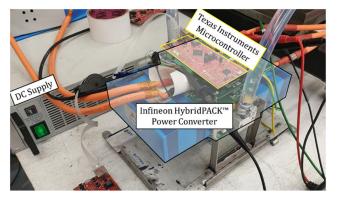Differentiating

Fig. 4 *Test drive used in the experiment*

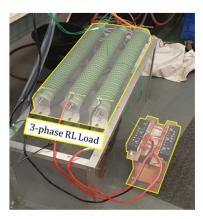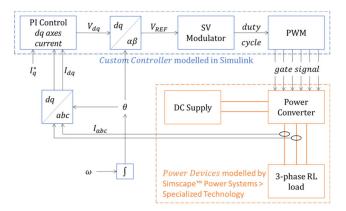**Fig. 5** *Passive three-phase RL load used in the experiment*

Fig. 6 *Schematic of an equivalent simulation model of test hardware*

$$\frac{\mathrm{d}x}{\mathrm{d}t} = \frac{\mathrm{d}\boldsymbol{C}(t)}{\mathrm{d}t}\boldsymbol{X} + \boldsymbol{C}(t)\frac{\mathrm{d}\boldsymbol{X}(t)}{\mathrm{d}t}$$

$$\simeq \begin{bmatrix} 1 & \cos\bar{\theta}(t) & \sin\bar{\theta}(t) & \cos\hat{\theta}(t) & \sin\hat{\theta}(t) \end{bmatrix}$$

$$\times \left(\begin{bmatrix} 0 & 0 & 0 & 0 & 0 \\ 0 & 0 & \bar{\omega}(t) & 0 & 0 \\ 0 & -\bar{\omega}(t) & 0 & 0 & 0 \\ 0 & 0 & 0 & 0 & \hat{\omega}(t) \\ 0 & 0 & 0 & -\hat{\omega}(t) & 0 \end{bmatrix} \begin{bmatrix} X_{0,0} \\ X_{0,1c} \\ X_{0,1s} \\ X_{1,0c} \\ X_{1,0s} \end{bmatrix} + \begin{bmatrix} \dot{X}_{0,0} \\ \dot{X}_{0,1c} \\ \dot{X}_{0,1s} \\ \dot{X}_{1,0c} \\ \dot{X}_{1,0s} \end{bmatrix} \right)$$

$$\simeq \boldsymbol{C}(t)\left(\boldsymbol{T}(t)\boldsymbol{X}(t) + \frac{\mathrm{d}\boldsymbol{X}(t)}{\mathrm{d}t} \right)$$

$$(19)$$

This shows that the model operation remains identical in the frequency domain with instantaneously changing $\boldsymbol{T}$. Its only during reconstruction in the time domain that $\boldsymbol{C}$ is treated properly as a function of θ and not directly from t.

4 Validation methodology

4.1 Experimental setup

An Infineon™-sourced IGBT-device full-bridge power converter was previously developed for a medium power (20 kW) racing application (University Formula Student Racing Team). The gate-driver circuit is controlled by a Texas Instruments™ microcontroller board running SVPWM modulation strategy with third harmonic injection, implemented through a custom control code. Full access to the control code was necessary that allowed tweaking the converter operation as required (Fig. 4).

A passive three-phase resistor–inductor (RL) load was used at the output instead of a physical permanent magnet synchronous motor (Fig. 5). This was done primarily to allow repeatability of experiments in controlled conditions, which would not have been possible with a real motor due to various mechanical issues (non-uniform shaft and loading on the shaft). Moreover, with an actual motor, the rotation (or fundamental frequency of operation) could not be directly controlled, especially with the heavy non-uniform shaft. Hence with the passive load, it was easy to artificially inject motor revolution per minute into the drive controller by hijacking the encoder signal.

Irrespective of the above limitations, this setup does not hamper the validity of the experiment. In an electric drive, most of the harmonics are introduced by the switching action in the inverter which is accounted for. Moreover, a simplistic RL load in the model and experimental setup albeit not a true representation of an electric machine is better in terms of purely validating the MFA model with a like-for-like comparison case. It is envisioned to build on these results to undertake real-life experiments in the very near future.

Lastly, the input filter was assumed to be absent ($L_f = 0$ and $C_f = \infty$) for this work due to the operation from a DC power supply. The authors' earlier work [1] has investigated the same model with the LC filter on the input side with good reconciliation with an equivalent switching model.

4.2 Equivalent simulation model

As an additional measure of validity and repeatability, a replica simulation model of the experimental setup was also built to account for the measurement errors and general noisy artefacts from various sources in physical experiments (Fig. 6). Care was taken to have this equivalent model as close to the physical operation as possible, i.e. solver parameters such as time-step, data-type, integration by accumulation were identical, the space vector modulation scheme was exactly copied in the equivalent model too by using the same look-up table for duty cycle computation.

4.3 Parameters used and frequency profile

The converter was driven by 200 V supply voltage and the switching frequency was set at 21 kHz. Two different configurations of the MFA model were used for comparisons

- MFA-1: DC component + fundamental component (variable) + third harmonic to fundamental (injected).
- MFA-2: above + switching (carrier) frequency.

R and L values per phase were determined experimentally to be 2 Ω and 3.5 mH. The resistance value is much higher than would normally be found in the stator winding of this class. The reason for choosing bigger resistors was to reduce the phase currents (limited by the maximum current capacity of DC supply) for the minimum level of input voltage required by the Infineon™ drive. The essential difference between this load and a generic AC machine stator winding is the absence of any back emf, which albeit is not a true representation but is legal for validation purposes.

A variable frequency profile (Fig. 7) was applied for a total duration of 1 s. The baseline electrical frequency of 600 Hz drops to 154 Hz over 200 ms and again rises to baseline. This is repeated three more times but with faster fall and rise ramps, doubling in every successive attempt. This validates linear frequency ramping of ±2230, ±4460, ±8920, and ±178,420 Hz/s. Careful observation
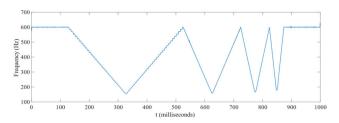
Fig. 7 *Frequency input waveform for open-loop experiments (experimental and simulation)*
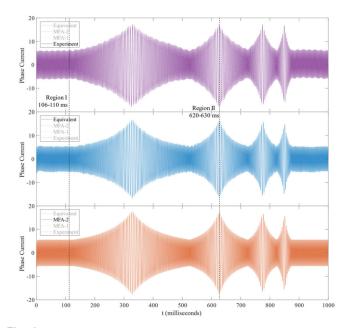

Fig. 8 *Current waveform comparison of the experimental, equivalent model, and MFA results for open-loop*

would reveal 'steps' in the frequency profile which was due to the way artificial injection of phase angle was implemented in the controller. Since the same frequency profile (with the discretisation artefact) was used for the MFA model and equivalent simulation model, this does not impact validation.

5 Benchmarking studies and results

Two sets of experiments were done:

- Open-loop: The proportional–integral (PI) controller was overridden by providing V_{dq} manually. Different sets of V_d and V_q were tested but only one set has been illustrated.
- Closed-loop: Current feedback was used to maintain a constant I_d (= 0) and I_q (= $k \cdot$ Torque) values.

Two phase currents were measured (balanced load condition with floating neutral deem third phase current measurement unnecessary), one has been shown in results.

5.1 Open-loop control

PI control was overridden to perform an open-loop test. $V_d = 0$ and $V_q = 0.5$ were set to produce the following.

It can be observed from the above that the current waveforms reconcile very well. Two different snapshots from Fig. 8 have been expanded in the following figures (Figs. 9 and 10) for better visual comparison with their respective frequency profiles (Figs. 11 and 12).

The time-domain plots for both high- and low-frequency regions show good reconciliation. A comparison of MFA with the equivalent model results would provide a more like-to-like comparison, excellent reconciliation is evident from the frequency plots too. Multiple harmonics of switching frequency could also be modelled using the MFA methodology but has not been done in this work. There is some amount of divergence from experimental results, most striking one is that the switching frequency phasor is overshooting both equivalent model and MFA model phasors by a significant margin. This can be characterised to various un-
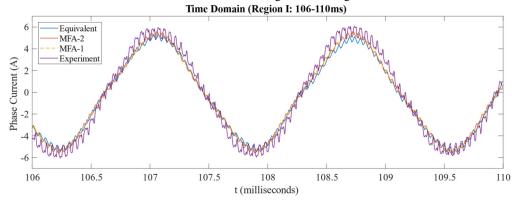

Fig. 9 *Current waveform comparison for region I, i.e. 106–110 ms. This region shows a fixed frequency of 600 Hz in open-loop operation*
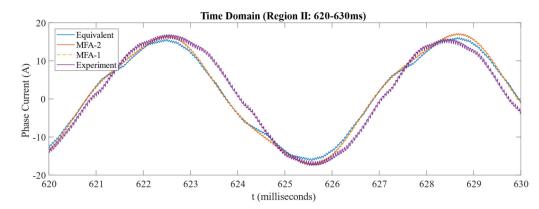

Fig. 10 *Current waveform comparison for region II, i.e. 620–630 ms. This region shows a fixed frequency of 154 Hz in open loop operation*
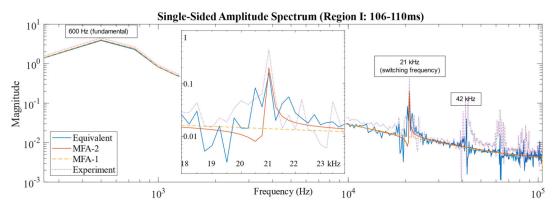
Fig. 11 *Frequency profile of phase current waveform for region I, i.e. 106–110 ms. Zoomed-in to highlight switching frequency region (inset)*
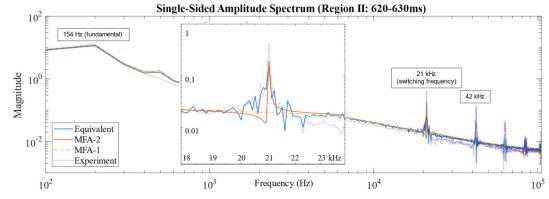

Fig. 12 *Frequency profile of phase current waveform for region II, i.e. 620–630 ms. Zoomed-in to highlight switching frequency region (inset)*
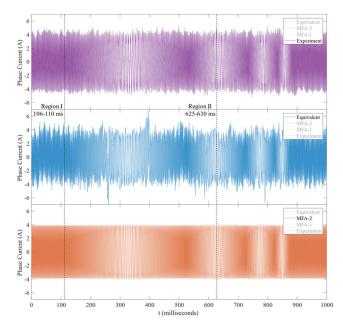

Fig. 13 *Current waveform comparison of experimental, equivalent model and MFA results for closed-loop*

modellable features of the hardware and measurement noise, evident from the fact that MFA and equivalent model plots are very close. The load parameters were approximated to fit the best RL series per-phase load and any deviation can be safely assumed to be caused by the non-ideal nature of inductance. This assumption is supported by the fact that the equivalent model waveform is in-line with the MFA.

5.2 Closed-loop PI control of quadrature current

Standard PI control was applied to currents in the *dq* axes. Gain values of P and I control were set at 630 and 210 (controller tuning beyond scope of this study and project), respectively. $I_d = 0$ and

$I_q = 4$ A was set for the controller. As before, two different snapshots from Fig. 13 have been zoomed in to demonstrate the model behaviour (Figs. 14 and 15). From initial visual inspection, it can be clearly seen that there is a lot of noise in the experimental and equivalent model waveforms which indicates badly tuned PI controller and/or significant noise in the feedback current signal to controller. The hardware controller is still under development and both the issues have been flagged.

The results show good reconciliation. In this case, no significant difference in MFA-1 and MFA-2 was observed. Most of the ripples seen in the waveforms are caused by the control action, i.e. current is rapidly oscillating between a small margin around the demanded current from the controller. As a consequence of the controller action, the frequency domain waveforms produced are non-legible and hence have not been reproduced in this study. The controller parameters are not tuned and are beyond the scope of this study.

A distinctly important advantage of the MFA model is that the control algorithm does not require any *abc–dq* or *dq–αβ* conversions since the coefficients of fundamental frequency sinusoids are the *d* and *q* components. Of course, if we have the controller in the modelling framework, reducing the simulation step size (to improve speed) would affect the controller bandwidth.

6 Conclusions

An important requirement in the automotive industry was identified, which could potentially reduce time and cost for hybrid powertrain development significantly. HIL simulation in automotive R&D has been essential since the past decade and with ever-improving communications and computing technologies, the concept of virtual simulation test-bed distributed across geographies is becoming more real than ever. This concept is already being explored for distributed grid applications globally, in an effort to build a global real-time super-grid [14, 15]. While the idea is similar, the application is significantly different for automotive traction, the latter being more dynamic with much faster transients.

In the effort of reaching a balance between high-fidelity waveforms and fast simulation speeds, the MFA modelling methodology was identified and explored in this work. A previous
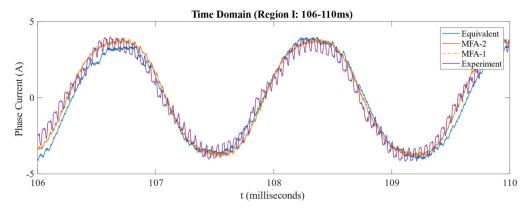
Fig. 14 *Current waveform comparison for region I, i.e. 106–110 ms. This region shows a fixed frequency of 600 Hz in closed-loop operation*
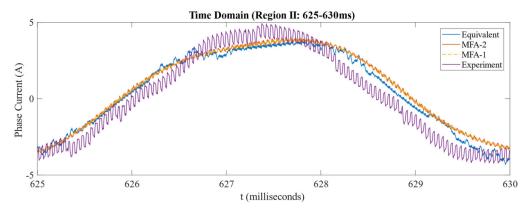

Fig. 15 *Current waveform comparison for region II, i.e. 625–630 ms. This region shows a fixed frequency of 154 Hz in closed-loop operation*

work by the authors [1] has demonstrated a simulation time reduction of up to 70% by employing various configurations of the MFA model. A survey of the literature did not, however, find a description of the MFA method applied to a variable frequency application. This study extended to a variable frequency MFA approach and carried out performance benchmarking of the model against experimental results from physical hardware.

Open-loop and closed-loop quadrature current control operations were performed, and phase current waveforms were compared. Notwithstanding the limitations in the experimental setup, the model showed substantially positive results. It was concluded that the non-ideal nature of any passive load can create divergence from an approximate model that may be minimised by modelling for the parasitic loads as well. Closed-loop control exponentially increases the 'un-modellability' of a power converter if not tuned properly.

As introduced in this study, the motivation is to have a remote observer model of an electric powertrain capable of predicting its baseline behaviour and be yielding to outlier events produced by the real hardware. This study marks an effort towards confirming a remote model capable of modelling the baseline behaviour. Operation in the frequency domain makes it much easier to exchange interface and state variables through dynamic phasors, which is the next step of the project.

7 Acknowledgement

8 References

[1] Sen, S., Evans, P.L., Johnson, C.M.: 'Multifrequency averaging (MFA) model of electric-hybrid powertrain suitable for variable frequency operation applied in geographically-distributed power hardware-in-the-loop (GD-PHIL) simulation'. 2018 IEEE Vehicle Power and Propulsion Conf. (VPPC), Chicago, 2018

[2] Östling, M., Salemi, A., Elahipanah, H., *et al.*: 'State of the art power switching devices in SiC and their applications'. IEEE Silicon Nanoelectronics Workshop (SNW), Honolulu, 2016

[3] Al-Hoor, W., Abu-Qahouq, J.A., Huang, L., *et al.*: 'Adaptive variable switching frequency digital controller algorithm to optimize efficiency'. 2007 IEEE Int. Symp. on Circuits and Systems, New Orleans, 2007

[4] Frances, A., Asensi, R., Garcia, O., *et al.*: 'Modeling electronic power converters in smart DC microgrids – an overview', *IEEE Trans Smart Grid*, 2018, **9**, (6), pp. 6274–6287

[5] Chiniforoosh, S., Jatskevich, J., Yazdani, A., *et al.*: 'Definitions and applications of dynamic average models for analysis of power systems', *IEEE Trans. Power Deliv.*, 2010, **25**, (4), pp. 2655–2669

[6] Davoudi, A., Jatskevich, J., Rybel, T.D.: 'Numerical state-space average-value modeling of PWM DC–DC converters operating in DCM and CCM', *IEEE Trans. Power Electron.*, 2006, **21**, (4), pp. 1003–1012

[7] Davoudi, A., Jatskevich, J., Chapman, P.L.: 'Computer-aided average-value modeling of peak current-mode controlled DC–DC converters considering parasites'. IEEE Power Electronics Specialists Conf., Orlando, 2007

[8] Bhejati, H., Niu, L., Davoudi, A., *et al.*: 'Alternative time-invariant multi-frequency modeling of PWM DC–DC converters', *IEEE Trans. Circuits Syst. I, Regul. Pap.*, 2013, **60**, (11), pp. 3069–3079

[9] Sanders, S., Noworolski, J., Liu, X., *et al.*: 'Generalized averaging method for power conversion circuits', *IEEE Trans. Power Electron.*, 1991, **6**, (2), pp. 251–259

[10] Lin, Z., Ma, H.: 'Modelling and analysis of three-phase inverter based on generalized state space averaging method'. IECON – 39th Annual Conf. of the IEEE Industrial Electronics Society, Vienna, 2013

[11] Liu, X., Cramer, A., Pan, F.: 'Generalized average method for time-invariant modelling of inverters', *IEEE Trans. Circuits Syst.*, 2016, **64**, (3), pp. 740–751

[12] Liu, X., Cramer, A.M.: 'Three-phase inverter modeling using multifrequency averaging with third harmonic injection'. 2016 IEEE Energy Conversion Congress and Exposition (ECCE), Milwaukee, 2016

[13] Ceschi, R., Gautier, J.-L.: '*Fourier analysis*' (John Wiley & Sons Inc., Hoboken, NJ, USA, 2017)

[14] Monti, A., Stevic, M., Vogel, S., *et al.*: 'A global real-time superlab: enabling high penetration of power electronics in the electric grid', *IEEE Power Electron. Mag.*, 2018, **5**, (3), pp. 35–44

[15] Stevic, M., Estebsari, A., Vogel, S., *et al.*: 'Multi-site European framework for real-time co-simulation of power systems', *IET Gener. Transm. Distrib.*, 2017, **11**, (17), pp. 4126–4135